



# The optical properties of urban aerosol in northern China: A case study at Xi'an



Chong-Shu Zhu<sup>a,b</sup>, Jun-Ji Cao<sup>a,b,d,\*</sup>, Kin-Fai Ho<sup>c,\*\*</sup>, L.-W. Antony Chen<sup>a,g</sup>, Ru-Jin Huang<sup>e</sup>, Yi-Chen Wang<sup>a</sup>, Hua Li<sup>a,h</sup>, Zhen-Xing Shen<sup>f</sup>, Judith C. Chow<sup>a,g</sup>, John G. Watson<sup>a,g</sup>, Xiao-li Su<sup>a</sup>, Qi-yuan Wang<sup>a</sup>, Shun Xiao<sup>a,i</sup>

<sup>a</sup> Key Laboratory of Aerosol Chemistry & Physics, Institute of Earth Environment, Chinese Academy of Sciences, Xi'an, China

<sup>b</sup> SKLLQG, Institute of Earth Environment, Chinese Academy of Sciences, Xi'an, China

<sup>c</sup> The Jockey Club School of Public Health and Primary Care, The Chinese University of Hong Kong, Shatin, Hong Kong

<sup>d</sup> Institute of Global Environmental Change, Xi'an Jiaotong University, Xi'an, China

<sup>e</sup> Laboratory of Atmospheric Chemistry, Paul Scherrer Institute (PSI), 5232 Villigen PSI, Switzerland

<sup>f</sup> Department of Environmental Science and Engineering, Xi'an Jiaotong University, Xi'an, China

<sup>g</sup> Division of Atmospheric Sciences, Desert Research Institute, Reno, NV, USA

<sup>h</sup> Key Scientific Research Base of Ancient Polychrome Pottery Conservation, SACH, Emperor Qin Shihuang's Mausoleum Site Museum, Xi'an, China

<sup>i</sup> Shaanxi Meteorological Bureau, Xi'an, China

## ARTICLE INFO

### Article history:

Received 26 September 2014

Received in revised form 6 March 2015

Accepted 15 March 2015

Available online 24 March 2015

### Keywords:

PAX

SSA

Scattering coefficient

Absorption coefficient

Xi'an

## ABSTRACT

Simultaneous measurements of particle scattering coefficient ( $B_{\text{scat}}$ ) and absorption coefficient ( $B_{\text{abs}}$ ) were conducted at Xi'an from mid-August to mid-October 2012 to estimate the particle single scattering albedo (SSA) and the Ångström coefficients in highly polluted urban air. The hourly averaged  $B_{\text{scat}}$  was  $272 \text{ Mm}^{-1}$  at 532 nm and  $82 \text{ Mm}^{-1}$  at 870 nm, while hourly averaged  $B_{\text{abs}}$  was  $31 \text{ Mm}^{-1}$  at 532 nm and  $19 \text{ Mm}^{-1}$  at 870 nm. Similar diurnal variations for  $B_{\text{scat}}$  and  $B_{\text{abs}}$  were observed between the two wavelengths. The averaged SSA was 0.88 at 532 nm and 0.78 at 870 nm. Based on the Ångström coefficients, anthropogenic fine particles show dominant contribution during the sampling period, accompanied by occasional dust events. Moreover, the major contributors to aerosol optical properties are attributed to the mixture of black carbon (BC) and brown carbon (BrC) with non-absorbing components over urban area in northern China. The findings provide useful insights into the factors affecting the visibility in northern Chinese cities and therefore essential knowledge for improving the air quality.

© 2015 Published by Elsevier B.V.

## 1. Introduction

The light extinction of aerosol particles, including scattering and absorption, affects visibility and climate (e.g., Ackerman et al., 2000; Watson, 2002; Jacobson, 2006; Koren et al., 2008; Ramanathan and Feng, 2009; Cao et al., 2012a). The scattering aerosol species such as sulfate and nitrate contribute to atmospheric cooling, while light absorbing aerosol species such as black carbon (BC), brown carbon (BrC) and dust exert a positive radiative forcing and reinforce the atmospheric warming due to an increase in the greenhouse gases (IPCC, 2007; Ramanathan and Carmichael, 2008).

The scattering coefficient ( $B_{\text{scat}}$ ) and absorption coefficient ( $B_{\text{abs}}$ ) are two important optical parameters describing the scattering and absorption cross sections in a unit volume of air at a wavelength of  $\lambda$ . These two optical parameters are important for modeling atmospheric radiation transfer (Clarke et al., 1987). The sum of  $B_{\text{scat}}$  and  $B_{\text{abs}}$  is the particle

extinction coefficient ( $B_{\text{ext}}$ ) determining the attenuation of light in the atmosphere, while the particle single scattering albedo (SSA) is defined as the ratio of  $B_{\text{scat}}/B_{\text{ext}}$  (Bodhaine, 1995):

$$\text{SSA} = B_{\text{scat}}/B_{\text{ext}} = B_{\text{scat}}/(B_{\text{scat}} + B_{\text{abs}}). \quad (1)$$

The wavelength dependence of SSA is determined by the size, chemical composition, and mixing state of particles (Kokhanovsky, 2008; Moosmüller et al., 2009; 2012). Though visibility and climate modeling should consider aerosol optical properties across the tropospheric solar spectrum (300–900 nm), SSA at mid-visible wavelength is often used to evaluate the aerosol radiative forcing. For example, Hansen et al. (1997) showed that a decrease of SSA at 550 nm from 0.9 to 0.8 may change the radiative forcing from negative (cooling) to positive (warming), depending on the surface albedo and aerosol optical depth. In general, the optical properties of atmospheric particles show a great spatial and temporal variability, due to the difference in concentration, particle size, chemical composition and mixing state (Kokhanovsky, 2008).

The urban areas in northern China are one of the most polluted regions in the world (e.g., Cao et al., 2012b; Zhang et al., 2013). However, direct measurements of aerosol optical properties in this region are very

\* Correspondence to: J.-J. Cao, Institute of Earth Environment, Chinese Academy of Sciences (CAS), No. 10 Fenghui South Road, High-Tech Zone, Xi'an 710075, China. Tel: +86 29 8832 6488; fax: 86 29 8832 0456.

\*\* Correspondence to: K.-F. Ho, The Jockey Club School of Public Health and Primary Care, The Chinese University of Hong Kong, Shatin, Hong Kong.

E-mail addresses: [cao@loess.llg.ac.cn](mailto:cao@loess.llg.ac.cn) (J.-J. Cao), [kfho@cuhk.edu.hk](mailto:kfho@cuhk.edu.hk) (K.-F. Ho).

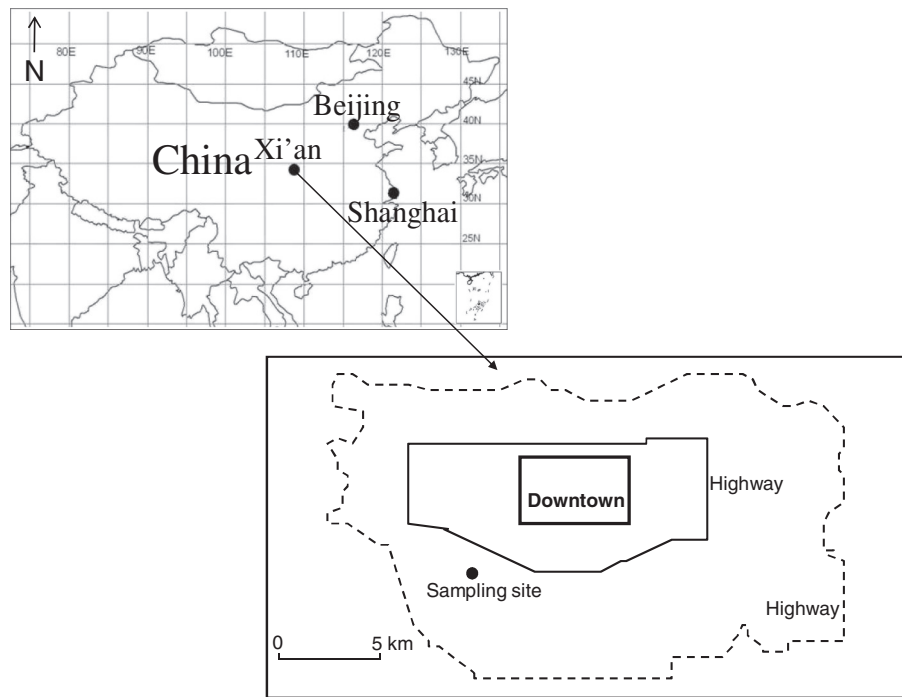


Fig. 1. Sampling location, Xi'an.

scarce to date, significantly hindering our understanding of the impact of aerosol on visibility and regional climate. Here, we present results of a 2-month field campaign carried out at Xi'an with a specific focus on aerosol scattering and absorption properties at both visible (532 nm) and near-infrared wavelengths (870 nm). The objectives of this study were: 1) investigating the variations of  $B_{\text{scat}}$ ,  $B_{\text{abs}}$ , and SSA, 2) establishing a conceptual equation for visibility degradation in Xi'an, and 3) estimating the main contributors to light extinction by using the Ångström coefficient.

## 2. Measurements

The measurements were conducted from mid-August to mid-October 2012 at the Institute of Earth Environment, Chinese Academy

of Sciences in Xi'an, China (Fig. 1). Xi'an is located on the Guanzhong Plain at the south edge of the Loess Plateau 400 m above sea level. Samples were taken on the roof of a two-story building ~10 m above ground level (34.23°N, 108.88°E), ~50 m west of a moderately traveled 4-lane round and ~25 m north of a lightly traveled 2-lane road. The monitoring site was located in an urban-scale zone of representation, where there are no major industrial activities (Cao et al., 2005). Xi'an is a megacity in northwestern China, characterized by high  $\text{PM}_{2.5}$  (particles with aerodynamic diameter  $\leq 2.5 \mu\text{m}$ ) pollution (Cao et al., 2012b). Coal combustion, biomass burning, vehicle emissions, and fugitive dust (airborne particles that originate from unpaved roads, agricultural cropland and construction sites) are reported to be the main contributors to the high particle pollution at this region (Cao et al., 2005, 2007, 2009; Shen et al., 2009). The average values of temperature, relative humidity

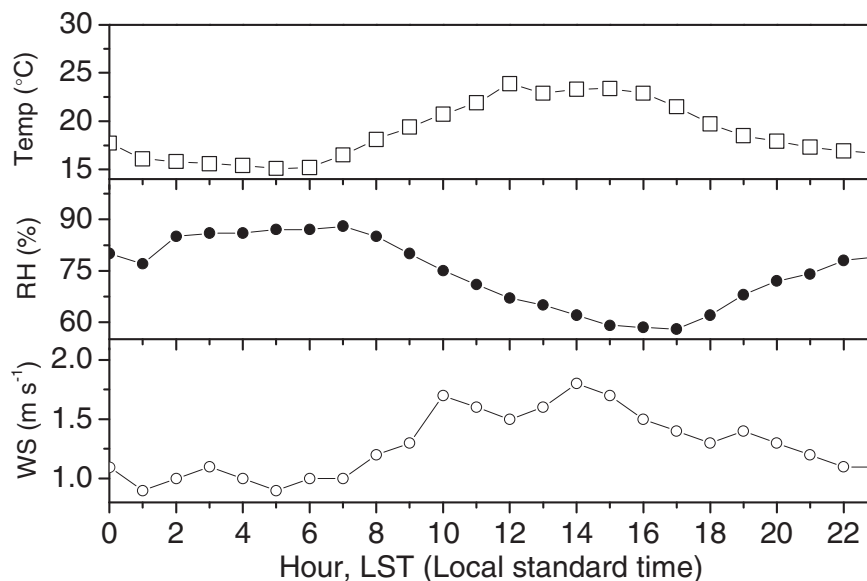
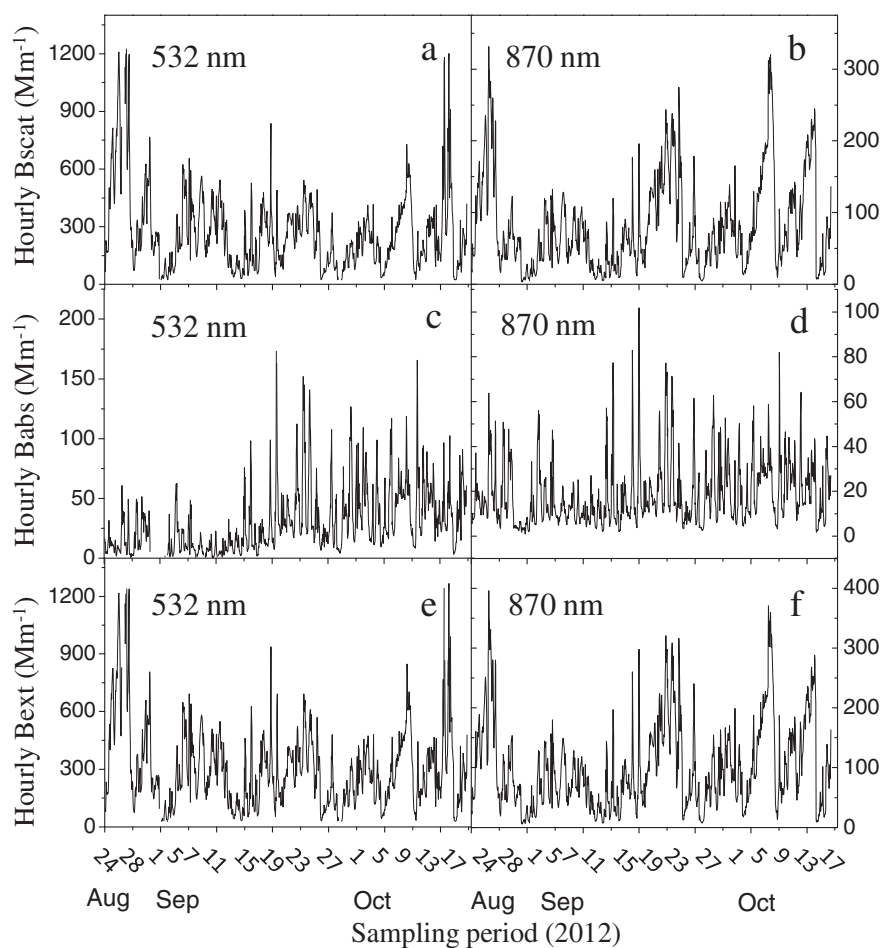


Fig. 2. Hourly average temperature (Temp), relative humidity (RH) and wind speed (WS) throughout the day during the sampling period.



**Fig. 3.** Hourly average values of: a) scattering coefficient ( $B_{\text{scat}}$ ) at 532 nm; b)  $B_{\text{scat}}$  at 870 nm; c) absorption coefficient ( $B_{\text{abs}}$ ) at 532 nm; d)  $B_{\text{abs}}$  at 870 nm; e) extinction coefficient ( $B_{\text{ext}}$ ) at 532 nm; f)  $B_{\text{ext}}$  at 870 nm.

(RH), and wind speed (WS) during the period are  $19 \pm 5$  °C,  $75 \pm 17\%$ , and  $1.3 \pm 0.8$  m s<sup>-1</sup>, respectively. These meteorological data are obtained from the Shaanxi Meteorological Bureau. Fig. 2 compares hourly average temperature, WS and RH throughout the day during the sampling period. Lower temperatures and wind speeds were observed in night-time than those for day-time, and the trend of relative humidity was inverse. The effects of meteorological conditions are discussed in the following sections.

PM<sub>2.5</sub> light scattering and absorption coefficients at 532 nm and 870 nm were measured using two Photoacoustic Extinctionmeters (PAX, Boulder, CO, USA), respectively (Kok et al., 2010; Wei et al., 2013). The PAX is a sensitive, high-resolution, fast-response instrument for measuring aerosol optical properties relevant for climate change and carbon particle sensing. The PAX uses a wide-angle integrating reciprocal nephelometer to measure the  $B_{\text{scat}}$ . The  $B_{\text{abs}}$  measurement uses in-situ photoacoustic technology. The scattering measurement responds to all particle types regardless of chemical makeup, mixing state, or morphology. Air flow at 1 L/min was drawn into the PAX and split to the nephelometer and photoacoustic resonator for simultaneous measurements of  $B_{\text{scat}}$  and  $B_{\text{abs}}$ . The nephelometer is based on a wide-angle (5 to 175°) reciprocal integration for light scattering with a detection limit (60-s average) of  $\sim 1$  Mm<sup>-1</sup>. The detection limit for photoacoustic detection of light absorption is also  $\sim 1$  Mm<sup>-1</sup>. The PAX uses a modulated diode laser (532 or 870 nm) as a common light source for nephelometer and photoacoustic sensor.

The calibrations for the PAX system are done before and after field campaigns according to the method recommended by DMT (Droplet Measurement Technologies, [www.dropletmeasurement.com](http://www.dropletmeasurement.com)), which

can reduce the system noise effectively. The procedures for calibrating the scattering and absorption measurements are described in PAX Operator Manual. The procedure includes data collection, data analysis and entering the new calibration coefficient. In this study, ammonium sulfate was used for both PAX scattering calibration, while the light absorptions were calibrated with NO<sub>2</sub> for PAX at 532 nm and freshly-generated propane soot for PAX at 870 nm. The calibration performed well for the present field campaign.

In this study,  $B_{\text{abs},870 \text{ nm}}$  is used as the surrogate for determining BC concentration (i.e., [BC]), as absorption from gases and non-BC aerosol species are relatively small at this wavelength. Measurements at 532 nm (green) represent the visible range at which the visual range (VR) is calculated. The  $B_{\text{abs},532 \text{ nm}}$  is then divided into two components, BC and non-BC. According to the previous studies (Bohren and Huffman,

**Table 1**

The minimum, maximum, average and standard deviations for  $B_{\text{scat}}$ ,  $B_{\text{abs}}$ ,  $B_{\text{ext}}$ , SSA, BC and VR at 532 nm and 870 nm.

Wavelength		$B_{\text{scat}}$ (Mm <sup>-1</sup> )	$B_{\text{abs}}$ (Mm <sup>-1</sup> )	$B_{\text{ext}}$ (Mm <sup>-1</sup> )	SSA	BC ( $\mu\text{g m}^{-3}$ )	VR (km)
532 nm	Min.	22	0.3	28	0.46	N.A. <sup>a</sup>	3.1
	Max.	1255	202	1269	0.99	N.A.	141.0
	Ave.	272	31	302	0.88	N.A.	12.9
	Stdev.	201	28	208	0.09	N.A.	23.3
870 nm	Min.	3	0.8	6	0.45	0.2	N.A.
	Max.	332	102	395	0.96	21.5	N.A.
	Ave.	82	19	101	0.78	3.9	N.A.
	Stdev.	64	14	73	0.11	3.0	N.A.

<sup>a</sup> No data.

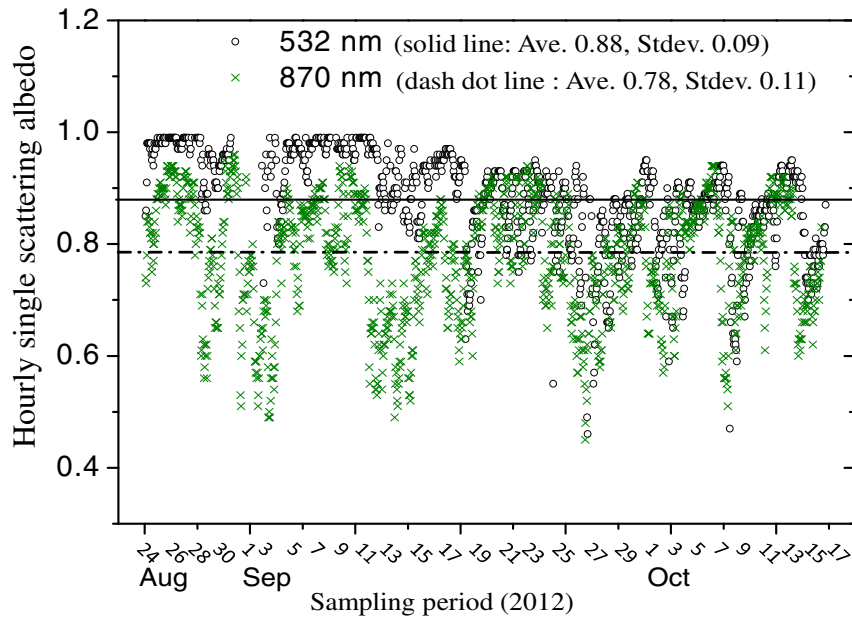


Fig. 4. Hourly average values of SSA at 532 nm and 870 nm, respectively.

1998; Bond, 2001; Gyawali et al., 2012), Eqs. (2) and (3) can calculate the contributions of BC and non-BC to  $B_{\text{abs},532 \text{ nm}}$ :

$$B_{\text{abs},532 \text{ nm}} = [\text{BC}] \times \sigma_{\text{BC},532 \text{ nm}} + B_{\text{abs},532 \text{ nm}}(\text{non-BC}). \quad (3)$$

$$B_{\text{abs},870 \text{ nm}} = [\text{BC}] \times \sigma_{\text{BC},870 \text{ nm}} \quad (2)$$

The BC mass-specific absorption cross-section ( $\sigma_{\text{BC}}$ ) is  $\lambda^{-1}$  dependent (Bond, 2001). The default values for  $\sigma_{\text{BC},870 \text{ nm}}$  and  $\sigma_{\text{BC},532 \text{ nm}}$  are

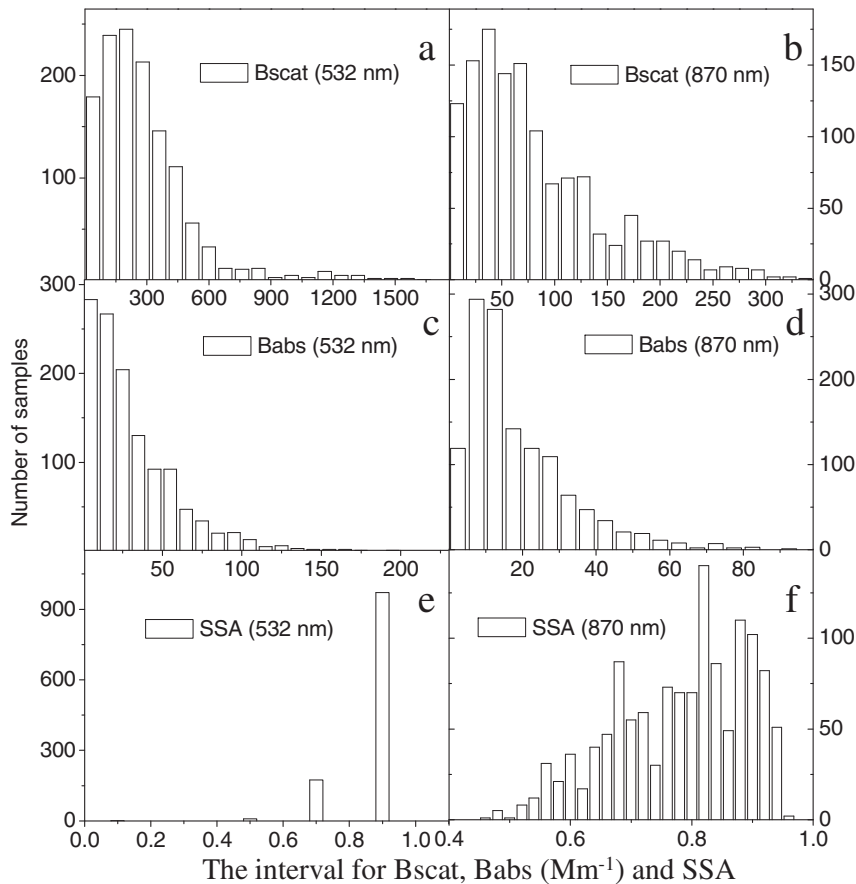


Fig. 5. Frequency histograms of: a) scattering coefficient ( $B_{\text{scat}}$ ) at 532 nm; b)  $B_{\text{scat}}$  at 870 nm; c) absorption coefficient ( $B_{\text{abs}}$ ) at 532 nm; d)  $B_{\text{abs}}$  at 870 nm; e) single scattering albedo (SSA) at 532 nm; f) SSA at 870 nm.

4.74 m<sup>2</sup> g<sup>-1</sup> and 7.75 m<sup>2</sup> g<sup>-1</sup>, respectively, recommended by the manufacturer. The value of  $\sigma_{BC}$  at 550 nm wavelength is reported as  $7.5 \pm 1.2$  m<sup>2</sup> g<sup>-1</sup> for fresh soot (Bond and Bergstrom, 2006a). Since  $\sigma_{BC}$  varies inversely with wavelength, and PAX has an 870 nm wavelength, the value of  $\sigma_{BC}$  for fresh soot is calculated.  $\sigma_{BC}$  can increase by as much as 50% depending on the mixing state (Bond and Bergstrom, 2006b). Note that if particles are more coated than the value of  $\sigma_{BC}$  reflects, then the PAX will overestimate BC mass. The default values for  $\sigma_{BC,870\text{ nm}}$  and  $\sigma_{BC,532\text{ nm}}$  are suitable and reasonable for an urban site. As [BC] is determined from Eq. (2), non-BC  $B_{abs,532\text{ nm}}$  can be calculated from Eq. (3). VR is estimated from  $B_{ext,532\text{ nm}}$  (Koschmieder, 1924a,b) following Eq. (4):

$$\begin{aligned} VR &= \frac{3.912}{B_{ext,532\text{ nm}}} \\ &= \frac{3.912}{(B_{abs,532\text{ nm}} + B_{scat,532\text{ nm}})} \\ &= \frac{3.912}{[B_{abs,532\text{ nm}}(BC) + B_{abs,532\text{ nm}}(\text{non-BC}) + B_{scat,532\text{ nm}}]} \end{aligned} \quad (4)$$

The Ångström coefficient (AC) is used to quantify wavelength dependence of aerosol light scattering (SAC) and absorption (AAC) coefficients from aerosols (Ångström, 1929; Flowers et al., 2010; Russell et al., 2010; Moosmüller et al., 2011). The two-wavelength AC is defined as:

$$\frac{p_1}{p_2} = (\lambda_1/\lambda_2)^{-AC} \quad (5)$$

where  $p_{\lambda_1}$  and  $p_{\lambda_2}$  can be scattering, absorption, or extinction coefficients at  $\lambda_1$  and  $\lambda_2$ , respectively. In this study, AC is determined by:

$$AC = -\frac{\ln\left(\frac{p_{532\text{ nm}}}{p_{870\text{ nm}}}\right)}{\ln\left(\frac{532}{870}\right)} = -\frac{\ln(p_{532\text{ nm}}) - \ln(p_{870\text{ nm}})}{\ln(532) - \ln(870)}. \quad (6)$$

SAC is strongly influenced by particle size, decreasing from 3–4 at the Rayleigh scattering limit (nanoparticles) to 0–1 at the large-particle limit (Seinfeld and Pandis, 1998), while AAC is less size dependent but affected by the relative contributions of BC, BrC and non-absorbing components. The extinction AC (EAC) is typically between SAC and AAC.

### 3. Results and discussion

#### 3.1. Variations of $B_{scat}$ , $B_{abs}$ , and SSA

The hourly average values of  $B_{scat}$ ,  $B_{abs}$  and  $B_{ext}$  show large variability during the study period (Fig. 3).  $B_{scat}$  vary over 60 folds, from 22 to 1255 Mm<sup>-1</sup> at 532 nm and over 100 folds from 3 to 332 Mm<sup>-1</sup> at 870 nm, while  $B_{abs}$  range from 0.3 to 202 Mm<sup>-1</sup> at 532 nm and from 0.8 to 102 Mm<sup>-1</sup> at 870 nm. Average  $B_{scat,532\text{ nm}}$  value of  $270 \pm 200$  Mm<sup>-1</sup> is higher than the average  $B_{scat,870\text{ nm}}$  value of  $82 \pm 64$  Mm<sup>-1</sup>. Average  $B_{abs}$  values are comparable, i.e.  $31 \pm 28$  Mm<sup>-1</sup> at 532 nm and  $19 \pm 14$  Mm<sup>-1</sup> at 870 nm. The average values of  $B_{ext}$  are  $300 \pm 200$  Mm<sup>-1</sup> and  $100 \pm 70$  Mm<sup>-1</sup> at 532 nm and 870 nm, respectively. The variations of  $B_{scat}$  and  $B_{abs}$  lead to a higher SSA at 532 nm ( $0.88 \pm 0.09$ ) than at 870 nm ( $0.78 \pm 0.11$ ) (Table 1). Hourly SSA also

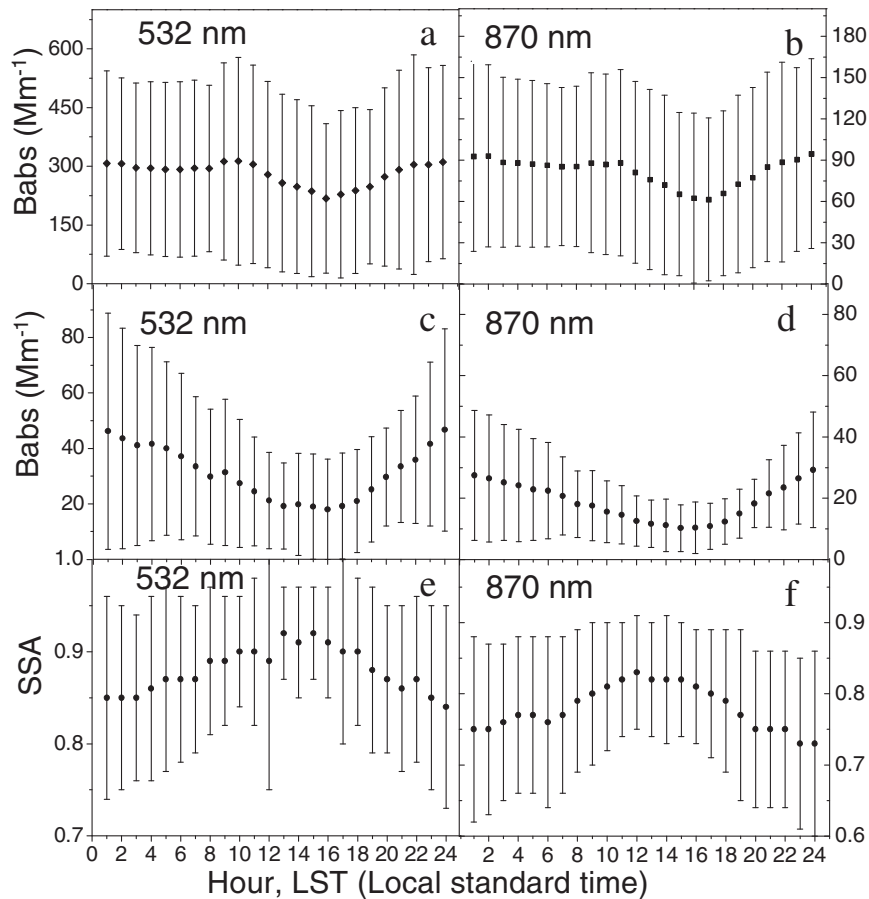


Fig. 6. Diurnal variations of: a) scattering coefficient ( $B_{scat}$ ) at 532 nm; b)  $B_{scat}$  at 870 nm; c) absorption coefficient ( $B_{abs}$ ) at 532 nm; d)  $B_{abs}$  at 870 nm; e) single scattering albedo (SSA) at 532 nm; f) SSA at 870 nm.

varied widely, from 0.46 to 0.99 at 532 nm and from 0.45 to 0.96 at 870 nm (Fig. 4).

The average  $B_{\text{scat},532 \text{ nm}}$  ( $270 \pm 200 \text{ Mm}^{-1}$ ) value obtained in the present study is comparable with the value ( $290 \pm 280 \text{ Mm}^{-1}$ ) observed in Beijing (He et al., 2009), but much lower than that at Guangzhou ( $420 \pm 160 \text{ Mm}^{-1}$ ) (Andreaea et al., 2008). While the average  $B_{\text{abs},532 \text{ nm}}$  ( $31 \pm 28 \text{ Mm}^{-1}$ ) value is much lower than those for Beijing ( $56 \pm 50 \text{ Mm}^{-1}$ ) and Guangzhou ( $91 \pm 60 \text{ Mm}^{-1}$ ) (He et al., 2009). Average SSA value of  $0.88 \pm 0.09$  at 532 nm in this study is higher than those at Beijing ( $0.80 \pm 0.09$ ) and Guangzhou ( $0.83 \pm 0.09$ ) (Andreaea et al., 2008; He et al., 2009). Even lower SSA in the mid-visible region are reported for megacities such as Shanghai (0.7, see Li et al., 2013) and Mexico City (0.68–0.73, see Marley et al., 2009). The results show that aerosols in the region are highly scattering resulted from non-absorbing components.

Higher percentage of  $B_{\text{abs}}$  to  $B_{\text{ext}}$  at 870 nm than that for 532 nm suggests the effect of diesel exhaust for the urban area. The results agree well with previous studies at Xi'an (Cao et al., 2005, 2007). Dubovik et al. (2002) reported that the SSA decreases with increasing wavelength for urban-industrial aerosols. For dust, SSA generally increases with wavelength attributing to the significant light absorbing at short wavelengths, while the tendency reverses for BC-rich aerosol from vehicular exhaust (Bergstrom et al., 2007; Gyawali et al., 2009; Sokolik and Toon, 1999). The present results of SSA decreasing with wavelength (0.88 at 532 nm and 0.78 at 870 nm) indicate that BC is a significant light absorber at Xi'an.

The frequency histograms of  $B_{\text{scat}}$ ,  $B_{\text{abs}}$  and SSA at 532 nm and 870 nm are shown in Fig. 5. The most frequent values of  $B_{\text{scat}}$  were  $200.0 \text{ Mm}^{-1}$  (19%) and  $37.5 \text{ Mm}^{-1}$  (14%), and for  $B_{\text{abs}}$   $5.0 \text{ Mm}^{-1}$  (23%) and  $7.5 \text{ Mm}^{-1}$  (22%) at 532 nm and 870 nm, respectively. Hourly average SSA values show the frequent peaks of 0.9 (84%) and 0.82 (11%) at 532 nm and 870 nm, respectively.

### 3.2. The diurnal variation of $B_{\text{scat}}$ , $B_{\text{abs}}$ and SSA

The diurnal variations at 532 nm and 870 nm show a similar pattern for  $B_{\text{scat}}$  and  $B_{\text{abs}}$  (Fig. 6).  $B_{\text{scat}}$  is almost constant between midnight and 10:00 LST, and reaches a minimum at around 16:00 LST and then gradually increases until midnight.  $B_{\text{abs}}$  exhibits strong diurnal variations with higher values at night and lower values during the day. Diurnal SSA ranged between 0.85 and 0.92 (with an average of 0.88) at 532 nm and between 0.73 and 0.83 (with an average of 0.78) at 870 nm (Fig. 6). The diurnal pattern of SSA showed a reversed pattern compared to  $B_{\text{abs}}$ , reaching the maximum (0.92 at 532 nm and 0.83 at 870 nm) around noon.

The diurnal variation of  $B_{\text{scat}}$  and  $B_{\text{abs}}$  in Xi'an reflects, to a certain extent, the traffic emissions, an intensification of midday turbulent mixing, and the formation of inversion layer after sunset (e.g., Gyawali et al., 2012). The  $B_{\text{abs}}$  peak value at 532 nm in early morning was about twice compared to the minimal value, while the enhancement was slightly smaller at 870 nm. Note that, biomass burning activities from rural area (usually occur at night) and heavy trucks (only permitted to pass through the urban area at night) can produce a large amount of BrC and BC, respectively. The surface inversion with the residual nocturnal layer aloft retained a few hours after sunrise, which results in vertical dispersion of primary pollutants. According to Fig. 2, the inverse trends between wind speed and  $B_{\text{abs}}$  were observed. Diurnal variation of SSA can also be explained by the increase of mixing layer depth and the decrease of  $B_{\text{abs}}$ . Mixing of secondary aerosol such as sulfate ( $\text{SO}_4^{2-}$ ) from aloft during midday and local nitrate ( $\text{NO}_3^-$ ) could also lead to enhanced SSA. The patterns of diurnal cycles are generally consistent with previous studies (He et al., 2009). The effects of meteorological conditions (e.g., temperature, wind speed, and relative humidity) on aerosol light properties are complicated, which is worth investigating in the future.

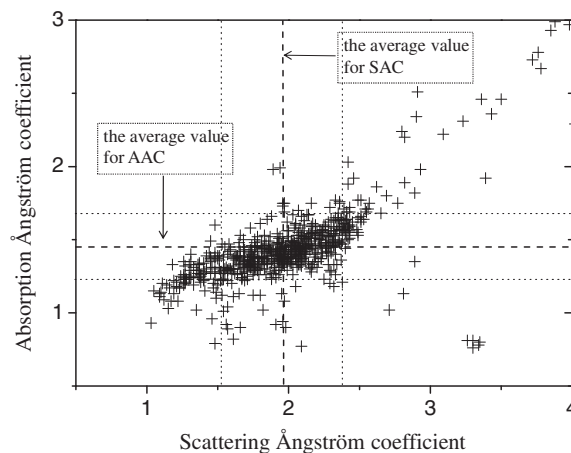


Fig. 7. Comparison of scattering Ångström coefficient (SAC) and absorption Ångström coefficient (AAC) calculated for Xi'an. The dashed lines are the average values for SAC and AAC, respectively.

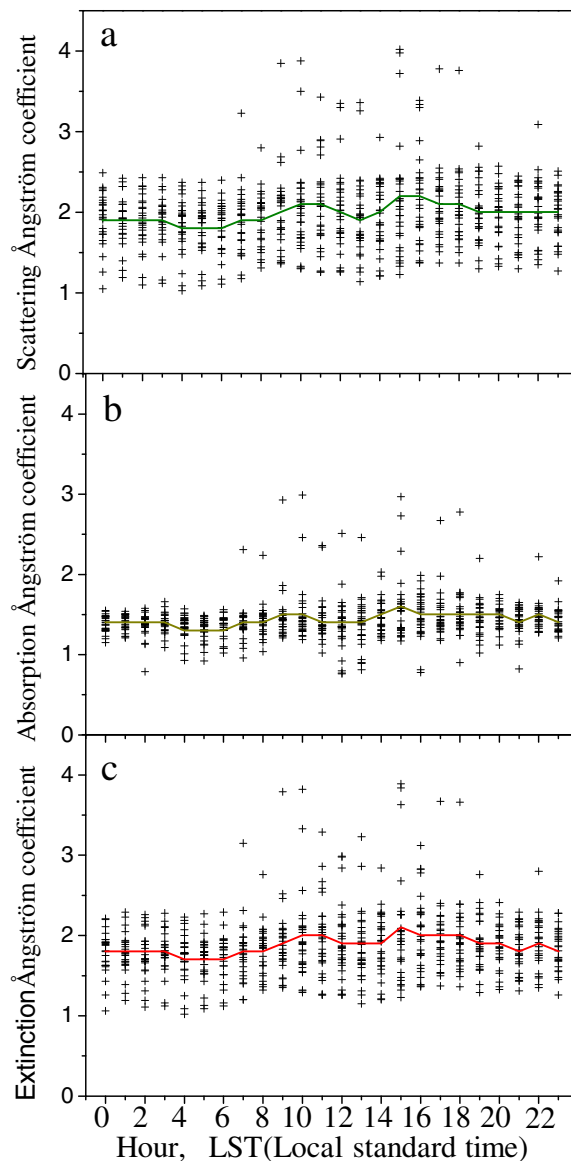
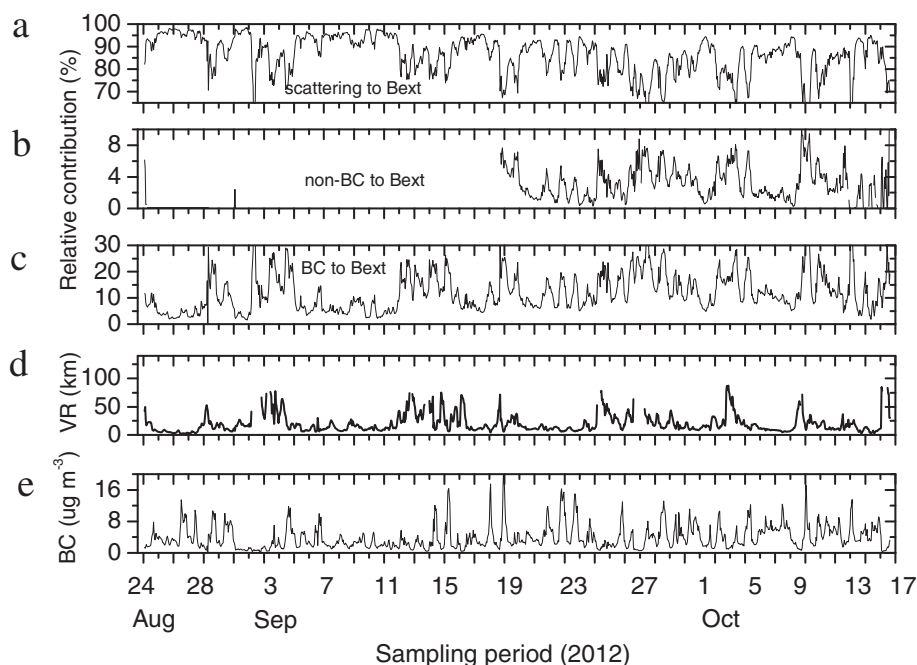


Fig. 8. Diurnal variations of: a) scattering Ångström coefficient (SAC); b) absorption Ångström coefficient (AAC); c) extinction Ångström coefficient (EAC).



**Fig. 9.** Hourly average values of: a) relative contribution of scattering to  $B_{\text{ext},532 \text{ nm}}$ ; b) relative contribution of non-BC to  $B_{\text{ext},532 \text{ nm}}$ ; c) relative contribution of BC to  $B_{\text{ext},532 \text{ nm}}$ ; d) visual range (VR) (km); e) the concentration of BC ( $\mu\text{g m}^{-3}$ ) at 870 nm.

### 3.3. Characteristics of SAC, AAC, and EAC

Comparison of hourly SAC and AAC is shown in Fig. 7. The dash lines are the average value for SAC and AAC, respectively. Based on Eq. (6), the Ångström coefficients were calculated using 532 nm and 870 nm wavelengths. The average values for SAC and AAC are  $1.98 \pm 0.45$  and  $1.43 \pm 0.25$ , respectively.

The SACs in the literature range from 0 for very large particles to 4 for very small particles, which is true for wavelength independent

refractive indices (Bohren and Huffman, 1998; Moosmüller and Arnott, 2009). For particles dominated by mineral dust, SAC is close to zero because the particles are mainly coarse particles with a larger scattering coefficient at larger wavelength (Yang et al., 2009; Schladitz et al., 2009; Sokolik and Toon, 1999). Fig. 7 shows that SAC values were higher than 1, which suggests the predominance of anthropogenic fine particles and few dust events during the sampling period.

AAC is often used to identify the contributions of non-BC (e.g., BrC and dust) to visible light absorption when describing the light absorption of aerosol components. AAC values in the present study ranging between 1 and 1.6 can be attributed to mixture of BC and non-absorbing particles and AAC higher than 1.6 can be associated with BrC (Lack and Cappa, 2010). Thus it seems that the average AAC value of 1.43 indicates the mixture of BC and BrC with non-absorbing components. Low AAC may be due to the abundance of BC of fossil fuel origin (Soni et al., 2010) and OC coatings. Previous researches reported that OC coatings (representing internal mixing) are found to change the AAC for BC from 0.7 (no coated) to 0.1 (all particles coated) (Gyawali et al., 2009; Chung et al., 2012; Bahadur et al., 2012).

The average EAC value of  $1.87 \pm 0.40$ , determined using Eq. (6), indicating a larger scattering coefficient at the shorter wavelength. The values of SAC and AAC determined here were comparable with a previous research (Yang et al., 2009). The results indicated the contributors to light extinction mainly attributing to BC, BrC and other non-absorbing components at Xi'an.

### 3.4. Diurnal variations of SAC, AAC and EAC

The diurnal variations of SAC, AAC and EAC exhibit similar variability and peak at 10:00 and 15:00 LST (Fig. 8). Lowest values are found during the early morning with 1.8, 1.3 and 1.7 for SAC, AAC and EAC, respectively. The morning peak average SAC, AAC and EAC are about 2.1, 1.5 and 2.0, respectively. The values decrease slightly around noon and increase again from 14:00 to 15:00 LST, and the maximum values of the peaks are 2.2, 1.6 and 2.1 for SAC, AAC and EAC, respectively.

Worthy to note, there are little differences between the lowest and highest values of SAC, AAC and EAC, indicating no significant diurnal variations in the predominating particle size and types. Compared to

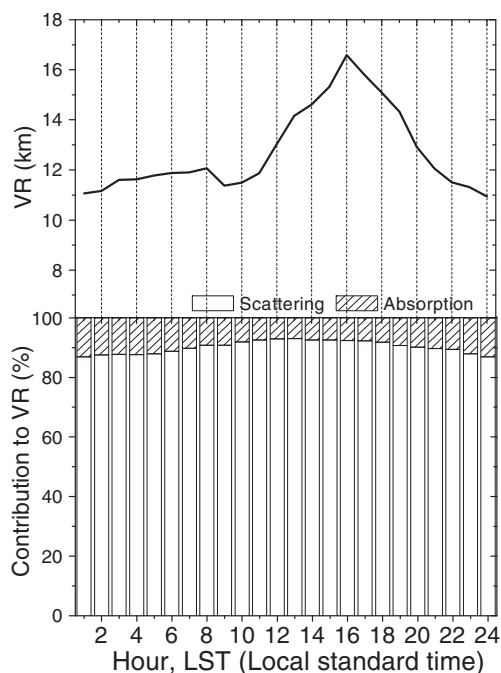


**Fig. 10.** Diurnal cycles of visual range (VR) (km) and the relative contributions of scattering and absorption to VR degradation.

AAC, SAC shows more variability (Fig. 8). SAC reaches the minimum in the early morning partly attributing to less local fresh emission. Lower SAC value around noon could be attributed to the boundary layer expansion and the enhanced photochemical secondary aerosol formation. The latter can lead to growth of particles to larger size via condensation and coagulation processes.

### 3.5. Visual range (VR) and apportionment of VR degradation

Fig. 9 shows the relative contributions of scattering, non-BC and BC to  $B_{\text{ext}}$ , the time series of hourly average VR (according to Eq. (4)) and BC concentrations during the study period. BC concentrations ranged from  $\sim 0.2$  to  $\sim 20.0 \mu\text{g m}^{-3}$  with an average of  $4.0 \mu\text{g m}^{-3}$ , accounting for 2–31% (average 12%) of  $B_{\text{ext},532 \text{ nm}}$ . The contribution of non-BC absorption to  $B_{\text{ext},532 \text{ nm}}$  is very small, ranging from 0 to 12.7% with an average of 1.7%. At this wavelength, optical absorption by BC is 7 times higher than that by non-BC. The rest of  $B_{\text{ext},532 \text{ nm}}$  is attributed to light scattering (ranged from 42 to 98% with an average of 86%). VR varied from  $\sim 3.1$  to  $\sim 141.0$  km with an average of 12.9 km during the study period.

Fig. 10 shows that the contribution of scattering to VR increased through the morning (8:00–10:00 LST) and reached the maximum (93.0%) at around 12:00–14:00 LST, which coincides with the highest SSA and VR (up to 17.0 km) during the day. The contribution of absorption to VR degradation is low, ranging from 6.9% to 13.8%. The lowest VR values range appeared during the morning rush hours. The results are comparable with the previous study (Cao et al., 2012a).

## 4. Conclusions

Aerosol optical properties in the megacity of Xi'an, China are studied. The  $B_{\text{scat}}$  average is  $272 \text{ Mm}^{-1}$  (ranging from 22 to  $1255 \text{ Mm}^{-1}$ ) at 532 nm, but decreases to  $82 \text{ Mm}^{-1}$  (ranging from 3 to  $332 \text{ Mm}^{-1}$ ) at 870 nm. Compared to scattering,  $B_{\text{abs}}$  is much lower with an average of  $31 \text{ Mm}^{-1}$  at 532 nm and  $19 \text{ Mm}^{-1}$  at 870 nm. The SSA at 532 nm (average 0.88) is higher than that at 870 nm (average 0.78), indicating that the light extinction is dominated by scattering. Diurnal variations of  $B_{\text{scat}}$ ,  $B_{\text{abs}}$ , and SSA are most likely determined by local anthropogenic sources, and meteorological conditions. The values of SAC (1.98), AAC (1.43) and EAC (1.87) show that the major contributors to aerosol optical properties are attributed to the mixture of BC and BrC with non-absorbing components. Our results suggest that reducing the non-absorbing components is likely to be important for improving the air quality over urban area in northern China.

## Acknowledgment

This study was supported by the National Natural Science Foundation of China (41230641, 41271481, 40925009), and projects from "Strategic Priority Research Program" of the Chinese Academy of Science (XDA05100401), Ministry of Science & Technology (201209007), and Shaanxi Government (2012KTZB03-01-01).

## References

Ackerman, A.S., Toon, O.B., Stevens, D.E., Heymsfield, A.J., Ramanathan, V., Welton, E.J., 2000. Reduction of tropical cloudiness by soot. *Science* 288, 1042–1047.

Andreaea, M.O., Schmida, O., Yang, H., Chand, D., Yu, J.Z., Zeng, L.M., Zhang, Y.H., 2008. Optical properties and chemical composition of the atmospheric aerosol in urban Guangzhou, China. *Atmos. Environ.* 42, 6335–6350.

Ångström, A., 1929. On the atmospheric transmission of sun radiation and on dust in the air. *Geogr. Ann.* 11, 156–166.

Bahadur, R., Praveen, P.S., Xu, Y., Ramanathan, V., 2012. Solar absorption by elemental and brown carbon determined from spectral observations. *Proc. Natl. Acad. Sci.* 109 (43), 17366–17371.

Bergstrom, R.W., Pilewskie, P., Russell, P.B., Redemann, J., Bond, T.C., Quinn, P.K., Sierau, B., 2007. Spectral absorption properties of atmospheric aerosols. *Atmos. Chem. Phys.* 7, 5937–5943.

Bodhaine, B.A., 1995. Aerosol absorption measurements at Barrow, Mauna Loa and the south pole. *J. Geophys. Res.* 100 (D5), 8967–8975.

Bohren, C.F., Huffman, D.R., 1998. *Absorption and Scattering of Light by Small Particles*. Wiley, New York (xiv, 530 pp.).

Bond, T.C., 2001. Spectral dependence of visible light absorption by carbonaceous particles emitted from coal combustion. *Geophys. Res. Lett.* 28, 4075–4078.

Bond, T.C., Bergstrom, R.W., 2006a. Light absorption by carbonaceous particles: an investigative review. *Aerosol Sci. Technol.* 40, 27–67.

Bond, T.C., Bergstrom, R.W., 2006b. Limitations in the enhancement of visible light absorption due to mixing state. *J. Geophys. Res.* 111, D20211. <http://dx.doi.org/10.1029/2006JD007315>.

Cao, J.J., Wu, F., Chow, J.C., Lee, S.C., Li, Y., Chen, S.W., An, Z.S., Fung, K.K., Watson, J.G., Zhu, C.S., Liu, S.X., 2005. Characterization and source apportionment of atmospheric organic and elemental carbon during fall and winter of 2003 in Xi'an, China. *Atmos. Chem. Phys.* 5, 3127–3137.

Cao, J.J., Lee, S.C., Chow, J.C., Watson, J.G., Ho, K.F., Zhang, R.J., Jin, Z.D., Shen, Z.X., Chen, G.C., Kang, Y.M., Zou, S.C., Zhang, L.Z., Qi, S.H., Dai, M.H., Cheng, Y., Hu, K., 2007. Spatial and seasonal distributions of carbonaceous aerosols over China. *J. Geophys. Res.* 112, D22511. <http://dx.doi.org/10.1029/2006JD008205>.

Cao, J.J., Zhu, C.S., Chow, J.C., Watson, J.G., Han, Y.M., Wang, G.H., Shen, Z.X., An, Z.S., 2009. Black carbon relationships with emissions and meteorology in Xi'an, China. *Atmos. Res.* 94, 194–202.

Cao, J.J., Wang, Q.Y., Chow, J.C., Watson, J.G., Tie, X.X., Shen, Z.X., Wang, P., An, Z.S., 2012a. Impacts of aerosol compositions on visibility impairment in Xi'an, China. *Atmos. Environ.* 59, 559–566.

Cao, J.J., Shen, Z.X., Chow, J.C., Watson, J.G., Lee, S.C., Tie, X.X., Ho, K.F., Wang, G.H., Han, Y.M., 2012b. Winter and summer  $\text{PM}_{2.5}$  chemical compositions in fourteen Chinese cities. *J. Air Waste Manage. Assoc.* 62 (10), 1214–1226.

Chung, C.E., Lee, K., Muller, D., 2012. Effect of internal mixture on black carbon radiative forcing. *Tellus Ser. B Chem. Phys. Meteorol.* 64, 1–13.

Clarke, A.D., Noone, K.J., Heintzenberg, J., Warren, S.G., Covert, D.S., 1987. *Aerosol light absorption measurement techniques: analysis and intercomparisons*. *Atmos. Environ.* 21, 1455–1465.

Dubovik, O., Holben, B., Eck, T.F., Smirnov, A., Kaufman, Y.J., King, M.D., Tanre, D., Slutsker, I., 2002. Variability of absorption and optical properties of key aerosol types observed in worldwide locations. *J. Atmos. Sci.* 59, 590–608.

Flowers, B.A., Dubey, M.K., Mazzoleni, C., Stone, E.A., Schauer, J.J., Kim, S.W., Yoon, S.C., 2010. Optical-chemical-microphysical relationships and closure studies for mixed carbonaceous aerosols observed at Jeju Island: 3-laser photoacoustic spectrometer, particle sizing, and filter analysis. *Atmos. Chem. Phys.* 10, 10387–10398. <http://dx.doi.org/10.5194/acp-10-10387-2010>.

Gyawali, M., Arnott, W.P., Lewis, K., Moosmüller, H., 2009. In situ aerosol optics in Reno, NV, USA during and after the summer 2008 California wildfires and the influence of absorbing and non-absorbing organic coatings on spectral light absorption. *Atmos. Chem. Phys.* 9, 8007–8015.

Gyawali, M., Arnott, W.P., Zaveri, R.A., Song, C., Moosmüller, H., Liu, L., Mishchenko, M.I., Chen, L.W.A., Green, M.C., Watson, J.G., Chow, J.C., 2012. Photoacoustic optical properties at UV, VIS, and near IR wavelengths for laboratory generated and winter time ambient urban aerosols. *Atmos. Chem. Phys.* 12, 2587–2601.

Hansen, J., Sato, M., Ruedy, R., 1997. Radiative forcing and climate response. *J. Geophys. Res.* 102, 6831–6864.

He, X., Li, C.C., Lau, A.K.H., Deng, Z.Z., Mao, J.T., Wang, M.H., Liu, X.Y., 2009. An intensive study of aerosol optical properties in Beijing urban area. *Atmos. Chem. Phys.* 9, 8903–8915.

Intergovernmental Panel on Climate Change (IPCC), 2007. *Climate change 2007: the scientific basis*. In: Solomon, S. (Ed.), *Contribution of Working Group I to the Fourth Assessment Report of the Intergovernmental Panel on Climate Change*. Cambridge Univ. Press, New York, p. 2007.

Jacobson, M.Z., 2006. Effects of externally-through-internally-mixed soot inclusions within clouds and precipitation on global climate. *J. Phys. Chem. A* 6860–6873.

Kok, G., Walker, J.W., Arnott, W.P., Arnold, J.J., Keady, P.B., 2010. Photoacoustic extinctions (PAX): a new instrument for measurement of climate-relevant optical properties of aerosols. AAAR 29th Annual Conference, Oregon Convention Center, Portland, Oregon, USA.

Kokhanovsky, A.A., 2008. *Aerosol Optics: Light Absorption and Scattering by Particles in the Atmosphere*. Springer-Praxis, Berlin.

Koren, I., Martins, J.V., Remer, L.A., Afargan, H., 2008. Smoke invigoration versus inhibition of clouds over the Amazon. *Science* 321, 946–949.

Koschmieder, H., 1924a. Theorie der horizontalen Sichtweite. *Beitr. Phys. Atmos.* 12, 33–53.

Koschmieder, H., 1924b. Theorie der horizontalen sichtweite II. Kontrast und Sichtweite (Theory of horizontal visibility). *Meteorol. Z.* 12, 171–181.

Lack, D.A., Cappa, C.D., 2010. Impact of brown and clear carbon on light absorption enhancement, single scatter albedo and absorption wavelength dependence of black carbon. *Atmos. Chem. Phys.* 10, 4207–4220.

Li, L., Chen, J., Wang, L., Melluki, W., Zhou, H., 2013. Aerosol single scattering albedo affected by chemical composition: an investigation using CRDS combined with MARGA. *Atmos. Res.* 124, 149–157.

Marley, N.A., Gaffney, J.S., Castro, T., Salcido, A., Frederick, J., 2009. Measurements of aerosol absorption and scattering in the Mexico City Metropolitan Area during the MILAGRO field campaign: a comparison of results from the T0 and T1 sites. *Atmos. Chem. Phys.* 9, 189–206.

Moosmüller, H., Arnott, W.P., 2009. Particle optics in the Rayleigh regime. *J. Air Waste Manag. Assoc.* 59, 1028–1031.

Moosmüller, H., Chakrabarty, R.K., Arnott, W.P., 2009. Aerosol light absorption and its measurement: a review. *J. Quant. Spectrosc. Radiat. Transf.* 110, 844–878.

- Moosmüller, H., Chakrabarty, R.K., Ehlers, K.M., Arnott, W.P., 2011. Absorption Ångström coefficient, brown carbon, and aerosols: basic concepts, bulk matter, and spherical particles. *Atmos. Chem. Phys.* 11, 1217–1225.
- Moosmüller, H., Engelbrecht, J.P., Skiba, M., Frey, G., Chakrabarty, R.K., Arnott, W.P., 2012. Single scattering albedo of fine mineral dust aerosols controlled by iron concentration. *J. Geophys. Res.* 117, D11210. <http://dx.doi.org/10.1029/2011JD016909>.
- Ramanathan, V., Carmichael, G., 2008. Global and regional climate changes due to black carbon. *Nat. Geosci.* 1, 221–227.
- Ramanathan, V., Feng, Y., 2009. Air pollution, greenhouse gases and climate change: global and regional perspectives. *Atmos. Environ.* 43, 37–50.
- Russell, P.B., Bergstrom, R.W., Shinzuka, Y., Clarke, A.D., De-Carlo, P.F., Jimenez, J.L., Livingston, J.M., Redemann, J., Dubovik, O., Strawa, A., 2010. Absorption Ångström Exponent in AERONET and related data as an indicator of aerosol composition. *Atmos. Chem. Phys.* 10, 1155–1169.
- Schläditz, A., Müller, T., Kaaden, N., Massling, A., Kandler, K., Ebert, M., Weinbruch, S., Deutscher, C., Wiedensohler, A., 2009. In situ measurements of optical properties at Tinfou (Morocco) during the Saharan Mineral Dust Experiment SAMUM 2006. *Tellus Ser. B Chem. Phys. Meteorol.* 61 (1), 64–78.
- Seinfeld, J.H., Pandis, S.N., 1998. *Atmospheric Chemistry and Physics: From Air Pollution to Climate Change*. Wiley, New York.
- Shen, Z.X., Cao, J.J., Arimoto, R., Han, Z.W., Zhang, R.J., Han, Y.M., Liu, S.X., Okuda, T., Nakao, S., Tanaka, S., 2009. Ionic composition of TSP and PM<sub>2.5</sub> during dust storms and air pollution episodes at Xi'an, China. *Atmos. Environ.* 43, 2911–2918.
- Sokolik, I.N., Toon, O.B., 1999. Incorporation of mineralogical composition into models of the radiative properties of mineral aerosol from UV to IR wavelengths. *J. Geophys. Res.* 104 (D8), 9423–9444.
- Soni, K., Singh, S., Bano, T., Tanwar, R.S., Nath, S., Arya, B.C., 2010. Variations in single scattering albedo and Angstrom absorption exponent during different seasons at Delhi, India. *Atmos. Environ.* 44 (35), 4355–4363.
- Watson, J.G., 2002. Visibility: science and regulation. *J. Air Waste Manage. Assoc.* 52 (6), 628–713.
- Wei, Y., Zhang, Q., Thompson, J.E., 2013. Atmospheric black carbon can exhibit enhanced light absorption at high relative humidity. *Atmos. Chem. Phys. Discuss.* 13, 29413–29445.
- Yang, M., Howell, S.G., Zhuang, J., Huebert, B.J., 2009. Attribution of aerosol light absorption to black carbon, brown carbon, and dust in China—interpretations of atmospheric measurements during EAST-AIRE. *Atmos. Chem. Phys.* 9, 2035–2050.
- Zhang, R.J., Jing, J.S., Tao, J., Hsu, S.C., Wang, G.H., Cao, J.J., Lee, C.S.L., Zhu, L., Chen, Z., Zhao, Y., Shen, Z.X., 2013. Chemical characterization and source apportionment of PM<sub>2.5</sub> in Beijing: seasonal perspective. *Atmos. Chem. Phys.* 13 (14), 7053–7074.